Building and Environment 59 (2013) 1–9

Contents lists available at SciVerse ScienceDirect

Building and Environment

journal homepage: www.elsevier.com/locate/buildenv

Numerical study of the effects of human body heat on particle transport and inhalation in indoor environment

Qinjiang Ge [a], Xiangdong Li [a], Kiao Inthavong [a], Jiyuan Tu [a,b,*]

[a] School of Aerospace, Mechanical and Manufacturing Engineering, RMIT University, PO Box 71, Plenty Road, Bundoora, VIC 3083, Australia
[b] Institute of Nuclear and New Energy Technology, Tsinghua University, PO Box 1021, Beijing 100084, China

ARTICLE INFO

Article history:
Received 2 May 2012
Received in revised form
18 July 2012
Accepted 2 August 2012

Keywords:
Body heat
Airflow field
Particle inhalation
Wind speed
CFD

ABSTRACT

The inhalation of micron particles by a manikin standing in a ventilated indoor environment was numerically investigated using Computational Fluid Dynamics (CFD). Computations were conducted with various combinations of the free stream velocity (0.05–0.25 m/s representing typical indoor wind speeds.), occupant orientation relative to the free stream (back-to-the-wind or facing-the-wind) and heat transfer (isothermal or thermal flow). It was found that the body heat has a significant impact on the airflow field in the vicinity of the manikin by causing an upwards airflow on the downstream side of the manikin. It was also found that the effect of body heat on particle inhalation depends on the manikin orientation relative to the free stream. When the manikin is facing-the-wind, body heat has a little effect on particle inhalation and can be neglected. However for a back-to-the-wind orientation, the situation is much more complicated as the source height of inhaled particles depends on the speed of free stream. When the wind speed is low (0.05 m/s), the critical area is located near the floor level. The central height of the critical area then increases with increasing free stream speed until it reaches the nose height when the wind speed rises up to 0.25 m/s. This indicates that the body heat is an important consideration when investigating contaminant inhalation by human occupants in low-speed (typically less than 0.2 m/s) indoor environment.

1. Introduction

The transport characteristics of aerosol particles and their inhalation characteristics by human occupants in indoor environments have been attached a great importance as people spend approximately 90% of their time indoors and a number of health problems have been found to be associated with particle inhalation [1]. During the past decades, numerous experimental and numerical investigations [2–7] have been conducted under various conditions. It is generally accepted nowadays that the particle inhalability by a human occupant is subjected to many factors such as the particle size, ambient wind speed, occupant movement, airflow pattern, inhalation rate, inhalation pattern (mouth or nasal inhalation), and even the human facial features.

However, most of the previous investigations on particle inhalation failed to take into account the effects of the metabolic heat released from a human body. In fact, a human body is continually exchanging energy with its environment. The average thermal energy generated by a human body with an ordinary activity level and at a moderate room temperature was found to be up to 100 W [8]. Due to this heat, a temperature gradient is formed and drives a buoyant convection in the vicinity of the human body, which is known as the *human thermal plume*. Homma and Yakiyama [9] measured the human thermal plume around a person standing in quiescent air using smoke wire photography and hot-wire anemometry. It was found that the thermal boundary layer was approximately 50 mm thick at the face level and its velocity was upto 0.25 m/s. Using a laser Doppler anemometer, Johnson et al. [10] measured the airflow around a human body standing with its back towards the free stream (0.2 m/s). A significant upward airflow was observed in the downstream side of the human body and the upward velocity was found to be approximately 0.19 m/s at the nose level. A synthetic literature survey demonstrated that the human thermal plume can produce vertical air velocities of 0.1–0.25 m/s in the breathing zone [9–12]. This vertical velocity induced by body heat is roughly equal to the average wind speed in most indoor environments (0.05–0.25 m/s according to Baldwin et al. [13] and Schmees et al. [14]), it is therefore reasonable to expect that the buoyancy-driven convection may change

* Corresponding author. School of Aerospace, Mechanical and Manufacturing Engineering, RMIT University, PO Box 71, Plenty Road, Bundoora, VIC 3083, Australia. Tel.: +61 3 9925 6191; fax: +61 3 9925 6108.
E-mail address: jiyuan.tu@rmit.edu.au (J. Tu).

0360-1323/$ – see front matter © 2012 Elsevier Ltd. All rights reserved.
http://dx.doi.org/10.1016/j.buildenv.2012.08.002

significantly the airflow pattern and play an important role in transporting aerosol particles in the vicinity of a human body. This is especially true for fine and ultrafine particles as their movement is mostly controlled by the indoor flow field [15].

During the past years, the effects of human thermal plume on aerosol particle transport and inhalation in quiescent air have been investigated by few researchers. For example, using a sedentary thermal manikin, Rim and Novoselac [12] experimentally investigated the effects of human thermal plume on the inhalability of fine/ultrafine particles in stratified indoor air. It was found that when the particle source was at floor level and in near proximity to an occupant, the inhaled particle concentration by the manikin was upto 4 times higher than the ambient concentration. This proved that the thermal plume plays an important role in transporting pollutants and particles from the floor level to the breathing zone. However, the conclusions based on quiescent or quasi-quiescent indoor air conditions may not be quantificationally applicable to realistic situations where ventilation is operating and the orientation of an occupant relative to the free stream may be random. Therefore, for the purpose of accurate description of the effects of human metabolic heat on particle transport and inhalation, some important factors including the wind speed and the occupant orientation relative to the wind have to be taken into account.

Therefore in this study, in order that the role of human body heat in particle transport and inhalation could be better understood, a series of CFD computations were conducted using a standing thermal manikin. Various factors including the wind speed (0.05–0.25 m/s), manikin orientation relative to the free stream (back-to-the-wind or facing-the-wind) and their combinations were investigated. For the purpose of comparison, computations with isothermal conditions were also performed. The predicted airflow field was in good agreement with the experimental data available in the literature. The trajectories of inhaled particles under various conditions were also presented and discussed. The outcome yielded from this study can help to reduce contaminant exposure through appropriate orientation arrangement in indoor environments.

2. Numerical methods

2.1. Geometric model and boundary conditions

The computational domain of this study was a rectangular wind tunnel containing a 1.6 m tall standing human manikin facing the $+X$ direction and with its nose tip in the plane of $X = 0$ m, as illustrated in Fig. 1. The dimensions of the computational wind tunnel (4 m-width $\times$ 7 m-depth $\times$ 3 m-height) were created large enough so that the flow field near the manikin was free from the effects of the no-slip condition of the stationary surrounding walls. In order that the detailed airflow pattern and particle transport characteristics in the breathing zone could be captured, the manikin head was carefully built to represent 50 percentage of a human male aged between 20 and 65 years [16]. For the purpose of saving computational cost, the manikin body was simplified. Unstructured tetrahedral and prism meshes were adopted to discretize the computational domain, with fine meshes around the manikin to capture the geometric features of the manikin and the effects of human thermal plume, as illustrated in Fig. 2. The grid sensitivity test proved that the mesh independence was achieved at 4.0 million cells, with the skewness of the cells and $y+$ value on the walls dropped below 0.8 and 0.78 respectively.

In total 21 cases were computed with various combinations of free stream speed, manikin orientation relative to the free stream and the status of heat transfer, as summarized in Table 1. For each computational case, evenly distributed airflow velocity profile was applied at the tunnel inlet and a zero pressure boundary condition was applied at the tunnel outlet. For the facing-the-wind cases, the inlet was on the $+X$ side and the outlet was on the $-X$ side of the tunnel, which makes the free stream flows in the $-X$ direction (Fig. 1). On the contrary, the inlet was on the $-X$ side and the outlet was on the $+X$ side of the tunnel for the back-to-the-wind cases, which makes the free stream flows in the $+X$ direction (Fig. 1). The free stream velocity was chosen to be in the range of 0.05–0.25 m/s, which represents the typical wind speeds in most indoor occupational environments [14]. The periodic respiration activities of the human body were neglected and the inhalation was assumed to be steady according to Horschler et al. [17]. A constant inhalation rate of 15 litres per minute (LPM) representing a human light breath at light activity conditions [7,18] was applied equally at the manikin nostrils, namely 7.5 LPM for each nostril.

For heat transfer modelling, the heat transfer between the air phase and the particle phase is neglected due to the dilute particle concentration. A constant free stream temperature of 26 °C, which is a typical air-conditioning ventilation temperature in summer seasons, was applied at the inlet and a constant temperature of 31 °C was applied at the manikin surface, as recommended by Gao and Niu [19]. The tunnel walls were assumed to be adiabatic.

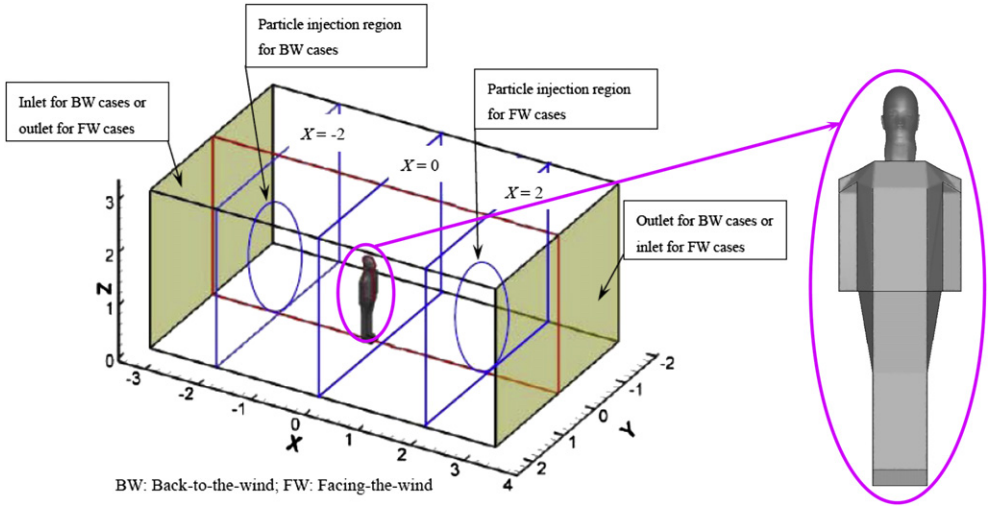

Fig. 1. The computational domain and human manikin.

Fig. 2. Refined meshes around the manikin model.

In order that the particle trajectories are fully developed before being affected by the thermal plume, particles with density of 1000 kg/m^3 are released from a circular region with 1.6 m diameter and located far away enough (2.0 m) from the nose tip plane. Namely, the particle release region is located in the $X = 2.0$ m plane for the facing-the-wind cases and in the $X = -2.0$ m plane for the back-to-the-wind cases (See Fig. 1). The particle size was chosen to be small enough (1.0 μm) so that the effect of gravitational settling could be neglected and the transport of particles is mostly controlled by the airflow field [20]. To achieve a uniform particle concentration assumption and to satisfy the "negligible bluff-off effects" criteria proposed by Chung et al. [21], the particles were released at the same velocity as that of the free stream.

Table 1
Computational cases.

Case no.	Wind speed (m/s)	Orientation	Type of flow	T_{inlet} (°C)	$T_{manikin}$ (°C)
1	0.05	Facing the wind	Isothermal	–	–
2	0.1				
3	0.15				
4	0.2				
5	0.25				
6	0.05	Facing the wind	Thermal	26	31
7	0.1				
8	0.15				
9	0.2				
10	0.25				
11	0.05	Back to the wind	Isothermal	–	–
12	0.1				
13	0.15				
14	0.2				
15	0.25				
16	0.05	Back to the wind	Thermal	26	31
17	0.1				
18	0.15				
19	0.2				
20	0.23				
21	0.25				

2.2. Flow and heat transfer models

The steady, incompressible Navier–Stokes equations are solved for the airflow field, where the continuity, momentum and energy equations are given in Equations (1)–(3), respectively.

$$\nabla\cdot\left(\rho\vec{U}\right) = 0 \tag{1}$$

$$\nabla\cdot\left(\rho\vec{U}\otimes\vec{U}\right) = \nabla\cdot(\mu+\mu_\tau)\left(\nabla\vec{U}+\left(\nabla\vec{U}\right)^T-\frac{2}{3}\delta_{ij}\nabla\cdot\vec{U}\right) - \nabla p + S_{buoy} \tag{2}$$

$$\nabla\cdot\left(\rho\vec{U}h\right) = \nabla\cdot(\lambda\nabla T)+\tau:\nabla\vec{U} \tag{3}$$

where, ρ, $\vec{U}$, p, h and T are density, velocity, pressure, enthalpy and temperature of the air, respectively. δ_{ij} is the Kronecher delta. μ and μ_τ are molecular and turbulent viscosity, respectively.$\tau:\nabla\vec{U}$ is the viscous dissipation. S_{buoy}, which represents the momentum source term due to the buoyancy force induced by the air temperature gradient, is defined by

$$S_{buoy} = -\rho_{ref}\beta\left(T-T_{ref}\right) \tag{4}$$

where, β is the thermal expansivity of air. ρ_{ref} and T_{ref} are the buoyancy reference density and temperature, which take values of the air density and temperature at the inlet, respectively.

The Re-Normalisation Group (RNG) k-ε model was chosen for the airflow turbulence because of its successful utilization in the simulations of indoor pollutant transport [22]. To resolve the boundary layer in the near wall regions, the Scalable Wall Function [23] was used. The pressure-velocity coupling was resolved using the SIMPLEC algorithm. The convective terms of the transport equations were discretized using second-order-upwind scheme in order to obtain sufficiently accurate solutions.

The particles are tracked through the air separately using the Lagrangian approach. There are many forces acting on a particle submerged in a continuous fluid, however, for micron particles with high density, the forces that depend on the density ratio are negligibly small [16]. Therefore, only the drag force $\vec{F}_D$ and the buoyancy force $\vec{F}_B$ are considered in this study and the equation of particle motion is given by

$$m_p\frac{d\vec{U}_p}{dt} = \vec{F}_D+\vec{F}_B \tag{5}$$

The drag force and buoyancy force are defined by

$$\vec{F}_D = \frac{1}{2}C_D\rho A_p\left|\vec{U}-\vec{U}_p\right|\left(\vec{U}-\vec{U}_p\right) \tag{6}$$

$$\vec{F}_B = (m_p-m)\vec{g} = \frac{\pi}{6}d_p^3(\rho_p-\rho)\vec{g} \tag{7}$$

where, m_p $\vec{U}_p$ and d_p are the particle mass, velocity and diameter, respectively, A_p is the projected particle area in the flow direction. The drag coefficient C_D is modelled by

$$C_D = \max\left(\frac{24}{Re}\left(1+0.15Re_p^{0.687}\right),0.44\right) \tag{8}$$

The above equations were solved in ANSYS CFX 12.1 using a segregated solver with an implicit formulation. The residual

values of the transport equations were set to converge at 10^{-5} or below for all simulation cases.

3. Results and discussion

3.1. Airflow field

The predicted airflow field was compared against Heist et al.'s [24] experimental data. In their experiments, Heist et al. [24] investigated the airflow pattern around a child-size manikin (80 cm in height, without breathing) standing with its back towards the coming free stream in a wind tunnel using laser Doppler anemometry. Particle transport was not included in the experiments. Heist et al.'s [24] experiments were conducted under isothermal and thermal conditions, respectively. In the isothermal condition, both the free stream and the manikin had the same temperature (21 °C) while in thermal condition, the temperatures of the free stream and the manikin surface were maintained at 21 °C and 33 °C, respectively. In order to achieve hydrodynamic and thermodynamic similarities with the experimental setup, boundary conditions of the CFD model were carefully chosen to produce an equal Reynolds number for the isothermal case and an equal Richardson number (Ri) for the thermal case, respectively, as listed in Table 2. The Richardson number is defined by

$$\mathrm{Ri} = \frac{\mathrm{Gr}}{\mathrm{Re}^2} = \frac{g\beta\left(T_s - T_{\mathrm{ref}}\right)H}{u^2} \tag{9}$$

where, Gr and Re are the Grashof number and Reynolds number, respectively. T_s is the manikin surface temperature, H is the manikin height and u is the velocity of the free stream.

The predicted airflow fields around the manikin under isothermal and thermal conditions are compared against the experimental results in Figs. 3 and 4, respectively. For the convenience of comparison, the coordinates in the figures are normalized with the manikin height (H).

Fig. 3 (a) and (b) illustrates the airflow velocity vectors in the symmetry plane of the manikin ($Y = 0$ m). It was found that under the isothermal conditions, a wake region containing two counter-rotating vortices is formed on the downstream side of the manikin. One of the vortices is larger and is located in the breathing zone while the other one is smaller and is located at a lower height (near the legs). The former vortex entrains air flowing around the head into the breathing zone. This suggests that aerosol contaminants that may be inhaled by an occupant are released from a source located at a height of the breathing zone. Similarly, due to the obstacle of the solid manikin, vortices are also observed in the horizontal planes. Fig. 3 (c) and (d) illustrates the airflow vectors in the horizontal plane of $Z/H = 0.6$, where two counter-rotating elliptic vortexes are distributed symmetrically on the downstream side of the manikin.

However, both the experiments and the numerical simulations under the thermal conditions presented a totally different figure of the airflow pattern. As illustrated in Fig. 4 (a) and (b), when heat transfer between the manikin and the air is included, the vortex region on the downstream side of the manikin (Fig. 3 (a) and (b)) is replaced by an upward rising airflow. Because of this rising airflow, the air in the breathing zone was observed to come from a lower height, especially from near the floor level, which indicates that the air and contaminants that may be inhaled are released from a source located near the floor. This difference makes the body heat an important consideration when locating the contaminant sources in actual situations. Meanwhile, the counter-rotating vortices in the horizontal plane of $Z/H = 0.6$ (Fig. 3 (c) and (d)) are significantly suppressed in the thermal condition, as illustrated in Fig. 4 (c) and (d).

Comparisons illustrated in Figs. 3 and 4 suggest that the simulated airflow fields generally agree well with the experimental results. The difference in the local vector distributions (Fig. 3 (a) and (b)) may be due to the different geometric shape of the manikins. More importantly, it is proved that due to the heat transfer between a human body and its surrounding air, there actually exists a distinct upward rising airflow on the downstream side of the body. Because of this rising airflow, air and particulate contaminants in the breathing zone that may be inhaled by a human occupant actually come from a lower level than that of the breathing zone. Therefore, for the purpose of effective assessment of particle transport and inhalation, the effect of human body heat has to be taken into account, which will be discussed in the following sections.

The airflow field was also validated using the CFD result of our previous study [7] which employed the same manikin model but different mesh arrangement, as shown in Fig. 5. An isothermal and thermal case under the facing-the-wind condition (Case 4 and Case 9 respectively) were chosen for the validation since they had the same wind speed and manikin orientation with those in our previous study [7]. The airflow velocity distribution along a vertical line which was 1 mm in front of the nose tip and had a length of 10 cm (the red vertical dot line starting at the chin height, see Fig. 5) was plotted and compared against King Se's [7] CFD results. For the convenience of comparison, the airflow velocity and the Z coordinate were normalized with the maximum velocity in this line and the length of the line, respectively. It was found that the predicted air velocity distribution was in a good agreement with our previously validated data. It also seemed that under facing-to-the-wind condition, the body heat has no obvious effects on air velocity distribution in the breathing zone. (For interpretation of the references to colour in this figure legend, the reader is referred to the web version of this article.)

3.2. Particle trajectories

As aforementioned, the affected region of body heat in a ventilated space is located at the downstream side of a human body. This indicates that when the manikin is facing the wind, the effect of body heat on particle inhalation is not significant since the airflow field in the breathing zone does not change significantly. Computations demonstrated that for the facing-the-wind cases, despite the totally different airflow field on the downstream side of the manikin, the tracks of inhaled particles are slightly different for the isothermal and thermal cases (Fig. 6). However, when the wind speed is low (typically lower than 0.1 m/s), the particle tracks on the upstream side of the manikin were observed to ascend in an isothermal case while slightly descending for a thermal case. Similar phenomena were also observed by Schmees et al. [14] in their visualization experiments of the airflow field around a thermal manikin standing in a wind tunnel (Fig. 6(b)), which had a similar thermo-hydrodynamic condition with that in this study. It was revealed that the ascending particle tracks in an isothermal case are due to the

Table 2
Experimental setup and boundary conditions of validation computations.

	u (m/s)	T_{ref} (°C)	T_s (°C)	H (m)	Re	Ri
Experiment-isothermal [19]	0.1	21	21	0.8	5481	–
Simulation-isothermal	0.051	21	21	1.6	5481	–
Experiment-thermal [19]	0.1	21	33	0.8	–	1.27
Simulation-thermal	0.051	21	22.6	1.6	–	1.27

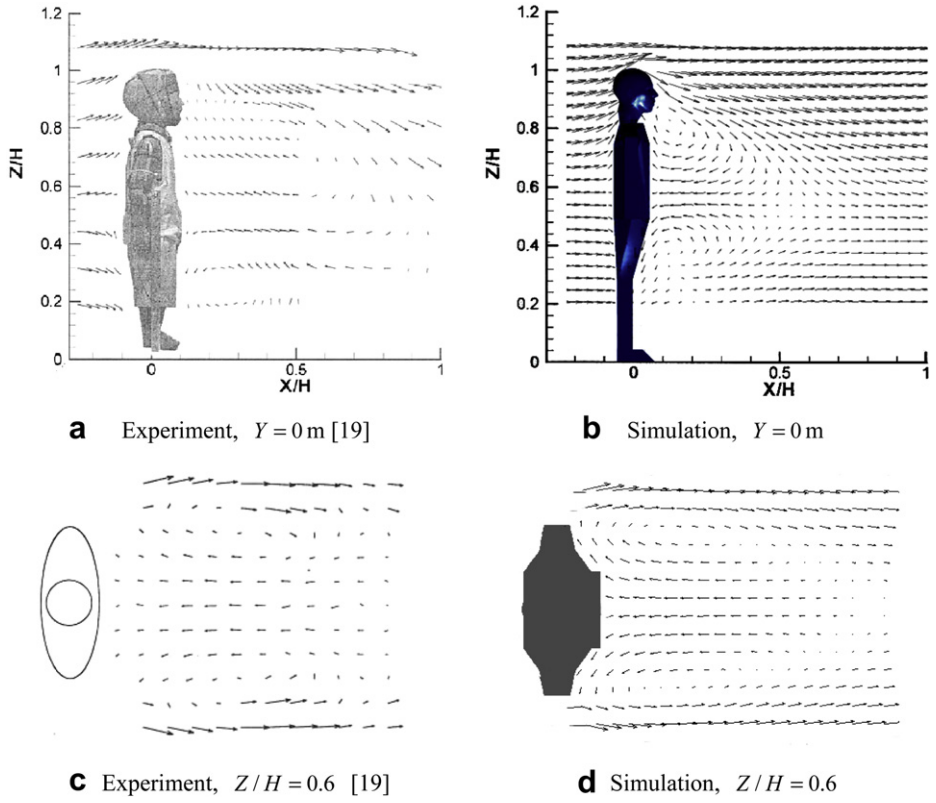

Fig. 3. Airflow velocity vectors under the isothermal condition.

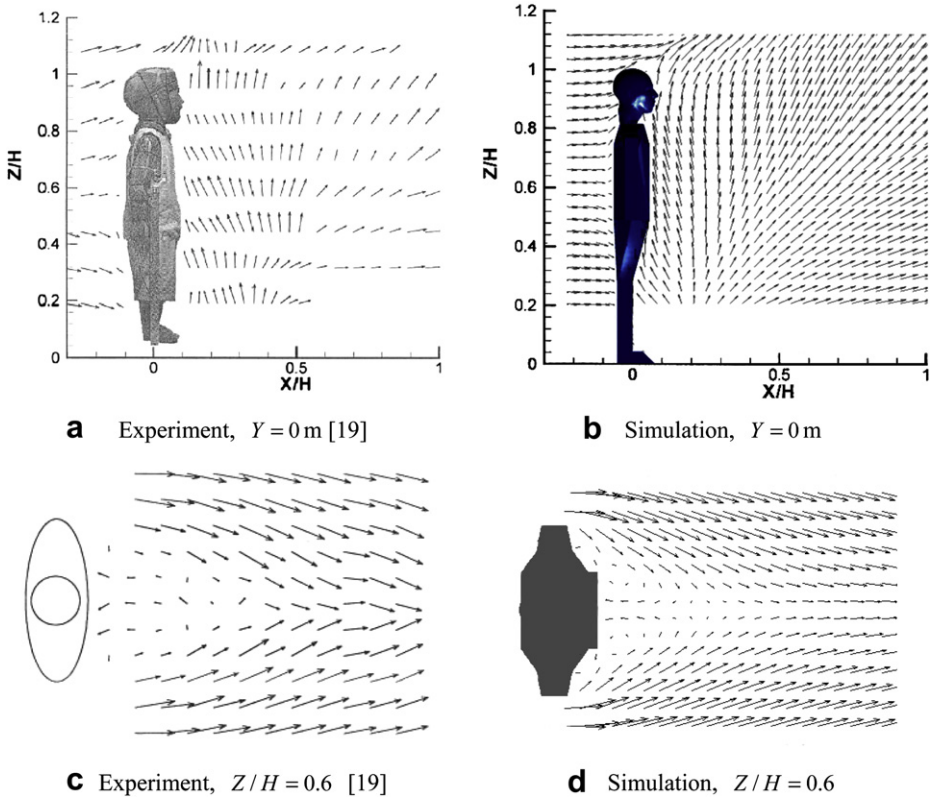

Fig. 4. Airflow velocity vectors under the thermal condition.

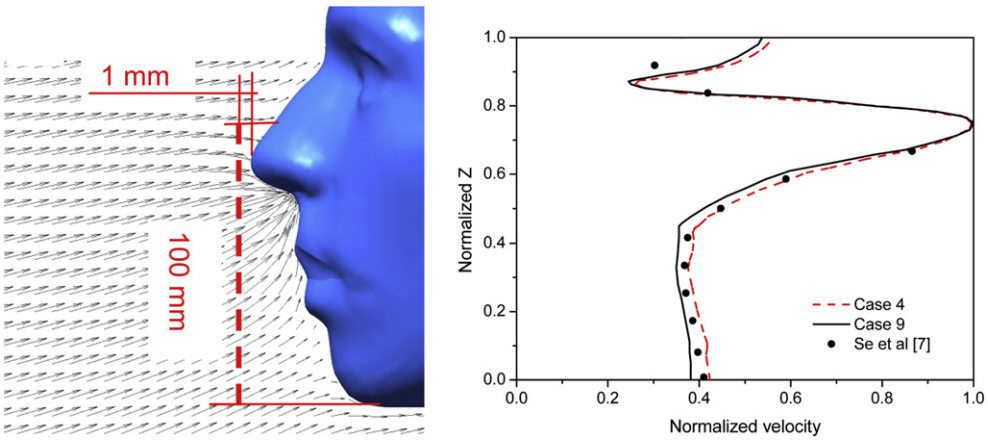

Fig. 5. Air velocity distribution in front of the nose tip.

rising airflow which bypasses the manikin while the descending particle tracks in a thermal case are associated with the body heat and the limited flow domain in the tunnel. As illustrated in Fig. 6(b), for a thermal manikin standing in a low-speed wind tunnel, the uprising airflow caused by the body heat forms a vortex flow when it reaches the top of the wind tunnel and is then mixed with the cold free stream. This vortex suppresses the oncoming airflow and causes a downward velocity. As a result of this, the airflow stream lines and the particle tracks upstream of the vortex are observed to descend. This vortex region is gradually eliminated with the increasing free stream speed. It was found that when the wind speed is larger than 0.2 m/s, no visible difference could be detected between the particle tracks predicted using the isothermal and thermal conditions, respectively.

On the other hand, when the manikin is back-to-the-wind oriented, computations presented totally different pictures of the tracks of inhaled particles for the isothermal and thermal cases, respectively. Fig. 7 illustrates typical airflow velocity vectors and tracks of inhaled particles under the isothermal and back-to-the-wind condition. It was found that when heat transfer is excluded from the CFD model, the predicted airflow field is similar to that shown in Fig. 3(b) and the inhaled particles are released from a source located at the breathing zone height and then passes the manikin head before being inhaled. It was also found that for the isothermal case, an increase in wind speed has no significant effect on the particle tracks and the airflow field profile.

Situations under the thermal and back-to-the-wind condition are much more complicated. Fig. 8 (a) illustrates that under the low wind-speed condition (0.05 m/s) and when heat transfer is included in the CFD model, a significant uprising airflow which is similar to that shown in Fig. 4 (b) is predicted and the particles being inhaled are actually released from a source located much lower than the breathing zone (near the floor level). As shown in Fig. 8 (a), particles approaching the manikin with the airflow bend their way upwards due to the buoyancy induced by the body heat. This is obviously different to what is shown in Fig. 7 but in good agreement with Rim's [12] experimental observations. In addition, it is also noticed that the uprising airflow on the downstream side of the manikin gradually develops into a vortex flow with increasing wind speed. With further increasing wind speed, the size of the vortex region increases in the horizontal direction while decreases in the vertical direction, as shown in Fig. 8 (b)–(d). Accordingly, particles go through a longer curved path before being inhaled due to the increased inertia. At the same time, it is noticed that another vortex with reverse rotation begins to appear and then expand its size and intensity at the manikin face height. The second vortex is formed due to the increased intensity of the free stream relative to the uprising airflow induced by the body heat. Computations proved that when the wind speed increases up to 0.23 m/s, particles released at the manikin face height, whose movement trajectories are not affected by the body heat, are also inhaled together with those released at a lower height whose tracks are controlled by the rising airflow (Fig. 8(c)). This indicates that the effect of body heat is suppressed by the increased wind speed. Finally, as the wind speed reaches 0.25 m/s (Fig. 8(d)), the thermal convection is not able to entrain particles into the breathing zone from the lower level so that only particles released at the face height are inhaled. A comparison of the airflow velocity vectors in Fig. 8(d) with those in Fig. 7 suggests that under such a high wind speed, body heat has only a neglectably weak effect on the airflow field.

3.3. The critical area

The particle tracks were further analysed using the so-called "critical area" concept, which is defined by Anthony et al. [2] as a finite area upstream of the breathing person where particles are inhaled. For the issue of this study, the critical area is located in the plane of particle injection (2.0 m upstream of the manikin). It was found that for the back-to-the-wind cases and when heat transfer was not included in the CFD model, the predicted critical areas (illustrated by solid marks in Fig. 9) were roughly located at the nose height and their dimensions were quite small. On the other hand when the body heat was taken into account, the predicted critical areas (illustrated by hollow marks in Fig. 9) were much larger but located at a lower height (around at the knee height). In addition, it was also noticed that the critical areas were roughly symmetrically distributed around the $Y = 0$ plane. This is physically reasonable since particles had to pass around the manikin (Fig. 8) before being inhaled. Under the thermal condition, the critical area shrank and moved upwards with increasing wind speed so that the body heat seemed to have no effect on particle inhalation when the wind speed reached 0.25 m/s as the critical area moved up to the nose height and overlapped the critical areas predicted using the isothermal conditions. This phenomenon makes it very crucial to take into account the body heat when investigating particle transport and inhalation in low-speed indoor environment.

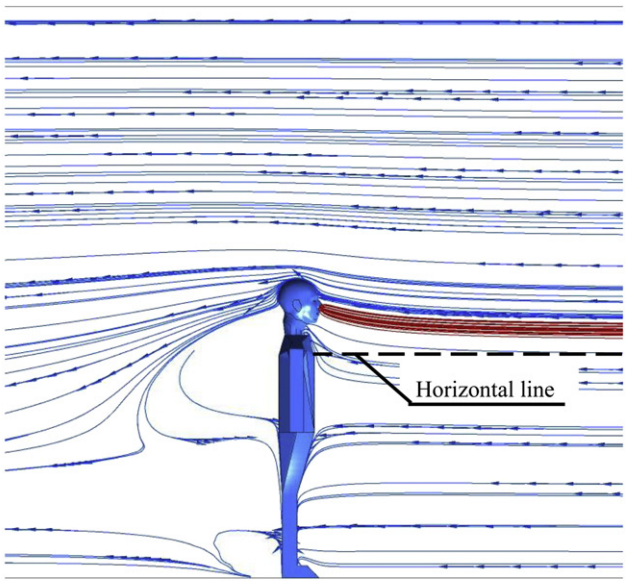

a Isothermal (Case 2, 0.10 m/s)

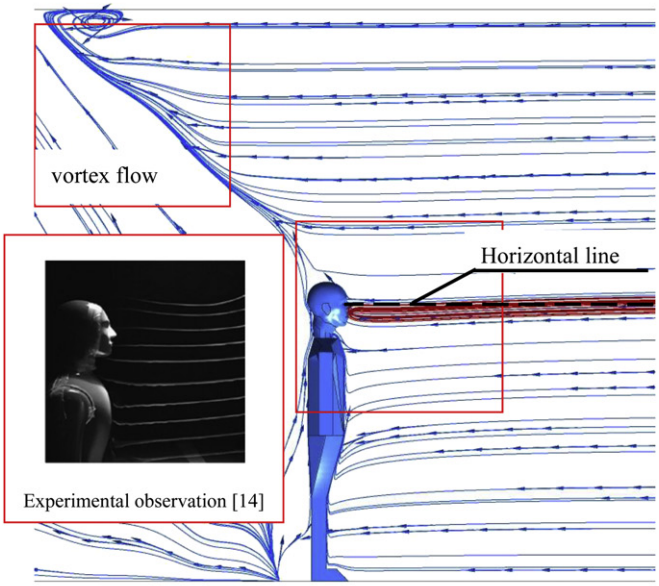

b Thermal (Case 7, 0.10 m/s)

Fig. 6. Particle tracks and stream lines in the facing-the-wind cases.

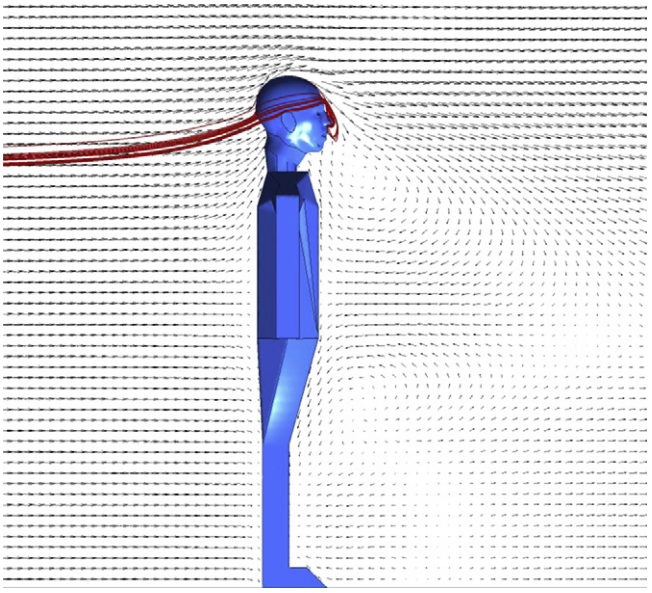

Fig. 7. Typical airflow field and particle tracks under the back-to-the-wind and isothermal condition (Case 15, 0.25 m/s).

For the purpose of further comparison, the central height of the critical areas under various conditions, including thermal and isothermal, as well as facing-the-wind and back-to-the-wind cases, are illustrated in Fig. 10. It is found that when the manikin is facing-the-wind and heat transfer is not included in the model, the wind speed has no effect on the central height of critical areas. When heat transfer is included in the facing-the-wind computations, the central height of critical area decreases gradually with increasing wind speed and finally approaches that of the isothermal cases. This phenomenon can be reasonably explained using Fig. 6 (b). In addition, when the manikin is back-to-the-wind and heat transfer is not considered, the predicted central height of critical area is still around the nose level, but slightly rises with increasing wind speed until approaching the horizontal lines representing the facing-the-wind and isothermal cases. However, the curve for the back-to-the-wind and thermal cases is totally different from the others. Fig. 10 illustrates that the central height of the critical area is quite low (typically near the floor) at low wind speed, then rises slightly with increasing wind speed. When the wind speed is larger than 0.2 m/s, the central height of critical area increases sharply because particles released at the nose height start to be inhaled. The portion of inhaled higher-level particles increases sharply so that when the wind speed approaches 0.25 m/s, no particles from the lower level could be inhaled and the effect of body heat on particle inhalation is totally suppressed.

Fig. 10 actually suggests that although the human metabolic heat has a significant effect on the airflow field in the vicinity of an occupant, its effect on particle inhalation is associated with the wind speed and the occupant-wind orientation. When an occupant is facing-the-wind, the particle tracks are slightly affected by the body heat and this effect is eliminated when the wind speed is over 0.2 m/s. However, when the occupant is back-to-the-wind, the inclusion of heat transfer in the CFD model leads to a totally different track distribution of inhaled particles. Similarly, it seems that the effect of body heat is largely suppressed as the wind speed is over 0.2 m/s. Despite this, for the purpose of effective modelling, human body heat remains an important consideration when investigating particle inhalation in indoor environment since the wind speed in most indoor spaces is lower than 0.25 m/s and the occupant-wind orientation may be random.

In summary, the effects of human body heat on particle inhalation can be summarized as follows: (1) When an occupant is facing the wind, the effects of body heat can be safely ignored since the affected region is located on the downstream side of the body. (2) When an occupant is oriented to be back-to-the-wind and the wind speed is lower than 0.2 m/s, the thermal plume caused by body heat plays an important role in transporting particle into the breathing zone from lower levels. However, even under the back-to-the-wind condition the effect of body heat on particle inhalation is gradually suppressed with increasing wind speed. As the wind speed rises up to 0.25 m/s, the effects of body heat on airflow

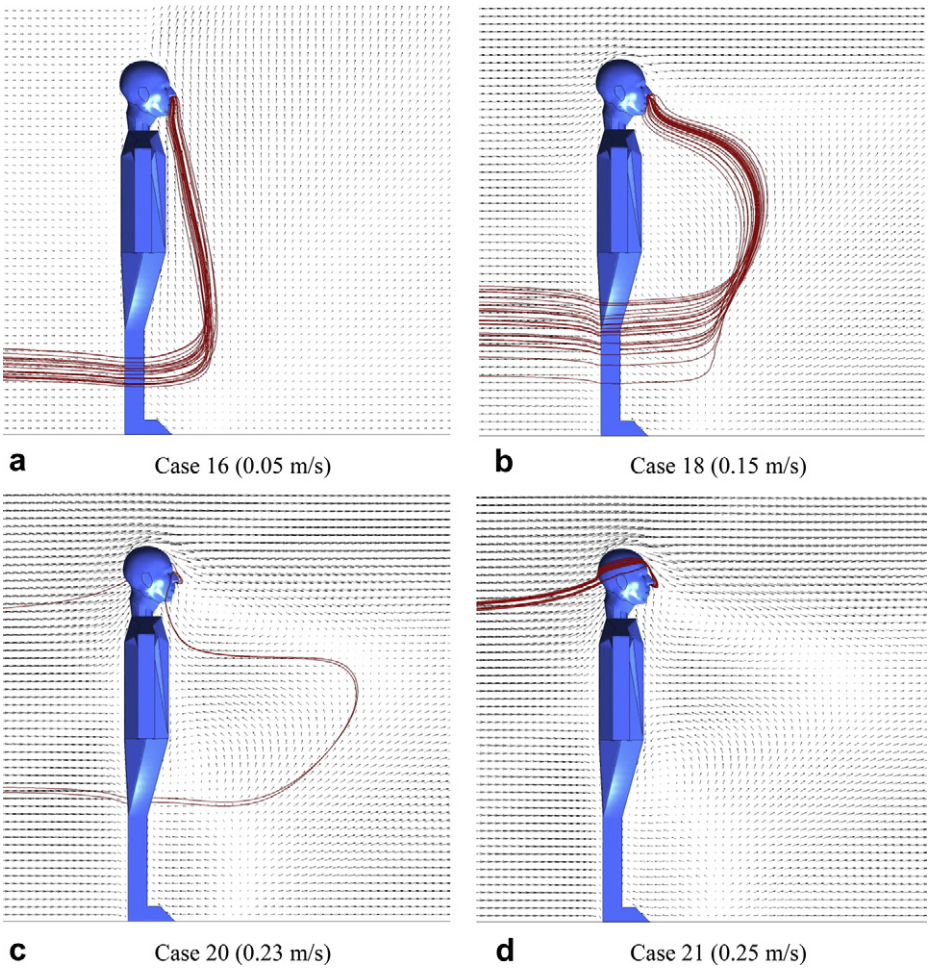

Fig. 8. Particle tracks under the thermal and back-to-the-wind condition.

field as well as particle transport and inhalation could not be detected and therefore could be ignored.

It should also be noted that since the average wind speed in most indoor environments is lower than 0.2 m/s according to the survey conducted by Baldwin and Maynard [13], the human body heat still remains an important consideration when investigating particle inhalation in indoor environment and assessing the health risks associated with particle inhalation.

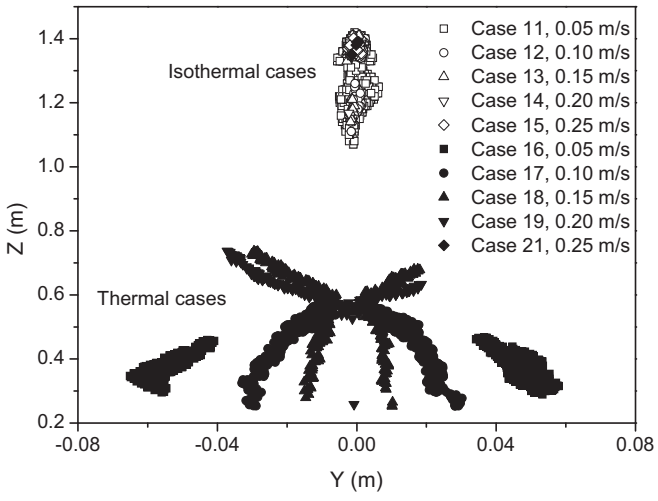

Fig. 9. Critical areas under the back-to-the-wind condition.

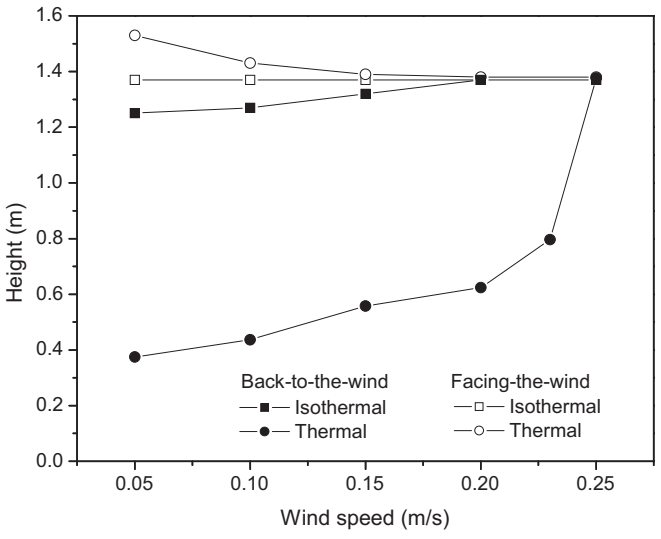

Fig. 10. Central height of the critical area vs. wind speed.

4. Conclusion

The effect of body heat on particle inhalation by a human manikin in a ventilated indoor environment was numerically investigated using CFD. Computations were conducted under both the facing-the-wind and back-to-the-wind conditions, as well as the isothermal and thermal conditions, respectively. Satisfactory agreement was obtained between the predicted airflow fields and the experimental observations available in the literature. The main conclusions arising from this study are as follows:

(1) For most indoor environments where the wind speed is lower than 0.2 m/s, the body heat causes a significant uprising airflow on the downstream side of the human body, which makes the occupant orientation relative to the free stream a crucial factor determining the importance of body heat on particle inhalation. When the occupant is facing-the-wind, the effect of body heat on particle inhalation could be safely neglected. However, when the manikin is back-to-the-wind, body heat plays an important role in transporting particles from near the floor level into the breathing zone.
(2) Although the effect of body heat is gradually suppressed by the increasing wind speed and this effect can be safely ignored when the wind speed is over 0.25 m/s, it still remains an important consideration when investigating particle transport and inhalation in most indoor environments where the wind speed is lower than 0.25 m/s.

Acknowledgements

The financial supports provided by the National Basic Research Program (973) of China (Grant No. 2012CB720100) and by the Australian Research Council (project ID LP110100140) are gratefully acknowledged.

References

[1] Inthavong K, Tian ZF, Tu JY. Effects of ventilation design on removal of particles in woodturning workstations. Build Environ 2009;44:125–36.
[2] Anthony TR, Flynn MR. Computational fluid dynamics investigation of particle inhalability. J Aerosol Sci 2006;37:750–65.
[3] Anthony TR, Flynn MR, Eisner A. Evaluation of facial features on particle inhalation. Ann Occup Hyg 2005;49:179–93.
[4] Aitken RJ, Baldwin PEJ, Beaumont GC, Kenny LC, Maynard AD. Aerosol inhalability in low air movement environments. J Aerosol Sci 1999;30:613–26.
[5] Hsu D-J, Swift DL. The measurements of human inhalability of ultralarge aerosols in calm air using mannikins. J Aerosol Sci 1999;30:1331–43.
[6] Hinds WC, Kennedy NJ, Tatyan K. Inhalability of large particles for mouth and nose breathing. J Aerosol Sci 1998;29(Suppl. 1):S277–8.
[7] King Se CM, Inthavong K, Tu J. Inhalability of micron particles through the nose and mouth. Inhal Toxicol 2010;22:287–300.
[8] Gowadia HA, Settles GS. Natural sampling of airborne trace signals from explosives concealed upon the human body. J Forensic Sci 2001;46:1324–31.
[9] Homma H, Yakiyama M. Examination of free convection around occupant's body caused by its metabolic heat. ASHRAE Trans 1988;94:104–24.
[10] Johnson AE, Fletcher B, Saunders CJ. Air movement around a worker in a low-speed flow field. Annu Occup Hyg 1996;40:57–64.
[11] Craven BA, Settles GS. A computational and experimental investigation of the human thermal plume. J Fluid Eng-T Asme 2006;128:1251–8.
[12] Rim D, Novoselac A. Transport of particulate and gaseous pollutants in the vicinity of a human body. Build Environ 2009;44:1840–9.
[13] Baldwin PEJ, Maynard AD. A survey of wind speeds in indoor workplaces. Ann Occup Hyg 1998;42:303–13.
[14] Schmees DK, Wu YH, Vincent JH. Visualization of the airflow around a life-sized, heated, breathing mannequin at ultralow windspeeds. Annu Occup Hyg 2008;52:351–60.
[15] Longest PW, Kleinstreuer C, Buchanan JR. Efficient computation of micro-particle dynamics including wall effects. Comput Fluids 2004;33:577–601.
[16] Li X, Inthavong K, Tu J. Particle inhalation and deposition in a human nasal cavity from the external surrounding environment. Build Environ 2011;47:32–49.
[17] Horschler I, Schroder W, Meinke M. On the assumption of steadiness of nasal cavity flow. J Biomech 2010;43:1081–5.
[18] Snyer WS, Cook MJ, Nasset ES, Karhausen LR, Parry Howells G, Tipton IH. Report of the task group on reference man. Pergamon Press; 1975.
[19] Gao N, Niu J. CFD study on micro-environment around human body and personalized ventilation. Build Environ 2004;39:795–805.
[20] Jiang J, Zhao K. Airflow and nanoparticle deposition in rat nose under various breathing and sniffing conditions–A computational evaluation of the unsteady and turbulent effect. J Aerosol Sci 2010;41:1030–43.
[21] Liu H, Zou C, Shi B, Tian Z, Zhang L, Zheng C. Thermal lattice-BGK model based on large-eddy simulation of turbulent natural convection due to internal heat generation. Int J of Heat and Mass Transfer 2006;49:4672–80.
[22] van Treeck C, Rank E, Krafczyk M, Tölke J, Nachtwey B. Extension of a hybrid thermal LBE scheme for large-eddy simulations of turbulent convective flows. Comput Fluids 2006;35:863–71.
[23] Mortensen M, Reif BAP, Wasberg CE. Assessment of the finite volume method applied to the V2F model. Int J Numer Methods Fluids 2010;63:495–516.
[24] Heist DK, Eisner AD, Mitchell W, Wiener R. Airflow around a child-size manikin in a low-speed wind environment. Aerosol Sci Technol 2003;37:303–14.